GROUND CLUTTER CANCELING WITH A REGRESSION FILTER

National Severe Storms Laboratory Interim Report

prepared by: Sebastián Torres

with contributions by: Dusan S. Zrnic and R. J. Doviak

October 1998

NOAA, National Severe Storms Laboratory

1313 Halley Circle, Norman, Oklahoma 73069

Table of Contents

1. Preface

This interim report documents part of accomplishments in the second year of the MOU with the Operational Support Facility. The report explores filtering of ground clutter in a staggered pulse repetition sequence. Specifically, a class of cancelers that use regression is examined. Thus, first an expose of regression filters is presented and then these are applied to a uniform PRT sequence. An extension to include staggered PRTs is made and tested. Results on a uniform PRT sequence are quite good but do not yet carry over to a staggered PRT. Approaches that might not degrade the spectral moment estimates of staggered sequences are proposed.

2. Introduction

Weather radar data is often contaminated with unwanted returns from the ground. Therefore, filtering techniques that attempt to ameliorate these signals are essential in nearly all Doppler radar systems. If the clutter is not at least partially removed, it mimics a meteorological signal and might produce strongly biased estimates of the three fundamental physical parameters (mean power, mean Doppler velocity, and spectrum width). In most cases, ground clutter signals have a very narrow spectrum width (long correlation time) and their mean Doppler velocity is zero. Thus, a high percentage of this interfering signal can be reduced if the spectral components in a band centered at zero frequency (zero Doppler velocity) are removed by using a suitable high-pass filter. Ground clutter filters with sharp narrow notches have been successfully designed and implemented in the WSR-88D to operate on uniformly spaced pulse trains, i.e. uniform pulse repetition time (PRT) (Heiss *et al*. 1990).

The mitigation of range-velocity ambiguities is an essential issue in Doppler weather radars and many efforts have been directed to the extension of the unambiguous velocity interval using variable PRT schemes. The use of non-uniform pulse spacing allows extension of the maximum unambiguous velocity by combining velocity estimates from two or more PRTs (Zrnic and Mahapatra, 1985). This improvement is related to the reciprocal of the difference of the underlying PRTs. Unfortunately, it has been accepted that the use of multiple PRTs (a non-uniform sampling process) is a principal obstacle for designing and implementing an effective ground clutter filter (Banjanin and Zrnic, 1991).

In this report, we address the issue of ground clutter elimination with regression filters. Besides being easily designed and implemented, these filters can be directly extended to signals that are not uniformly sampled. We begin by introducing the concept of multiple PRTs and its impact on the pulse-pair processor statistical performance. Then, some concepts of clutter filtering are presented with particular emphasis on implementation of such filters using regression filters. Once the design variables are described and analyzed, the regression filter performance on both uniform and staggered sample sequences is assessed. This is accomplished by studying statistical properties of

spectral moments of simulated weather signals to which ground clutter is superposed. Finally, a regression filter and a recursive filter designed for the NEXRAD are applied to a time series collected by an operational WSR-88D. After the conclusions, variations to the staggered PRT scheme are proposed for future work.

3. Variable PRT Processing

With the variable PRT technique, a velocity estimate v_i is obtained from echo samples spaced by T_i seconds, where the subscript i identifies each PRT in the scheme. These velocity estimates can be properly combined so that an estimate of the true velocity is obtained. To derive these estimates let us begin with the expression for a discrete-time representative autocorrelation of weather signals (Doviak and Zrnic, 1993)

$$R(mT_s) = S\exp[-8(\pi\sigma_v mT_s/\lambda)^2]e^{-j4\pi vmT_s/\lambda} + N\delta_m . \qquad (1)$$

In this equation, S is the mean power, v the mean velocity, σ_v the spectrum width, and T_s the sampling interval. In a multiple PRT scheme with n underlying PRTs (Fig. 1) we can estimate the lag-1 autocorrelation (m = 1) corresponding to each T_i as

$$R(T_i) = \frac{1}{K}\sum_{k=0}^{K-1} R^{(k)}(T_i) = \frac{1}{K}\sum_{k=0}^{K-1}\left[V^*(kT_o + \sum_{j=1}^{i-1} T_j)\cdot V(kT_o + \sum_{j=1}^{i} T_j)\right] ; \quad i = 1, 2,..., n \qquad (2)$$

where K is the number of batches of the basic PRT sequence, n is the number of T_i's in the sequence, $T_o = \sum_{i=1}^{n} T_i$ is the period of repetition or length of the basic PRT sequence, and M_T=Kn+1 is the total number of samples available to estimate each of the spectral moments. The symbol * denotes complex conjugation.

Then, from Eqs. (1) and (2), estimates of S, v and σ_v can be obtained as follows

$$\hat{S} = \frac{1}{M_T}\sum_{k=0}^{K-1}\sum_{i=1}^{n}\left| V(kT_o + \sum_{j=1}^{i-1} T_j)\right|^2 \qquad (3.a)$$

$$\hat{v} = \frac{\lambda}{4\pi(n-1)} \sum_{i=1}^{n-1} \frac{1}{(T_{i+1} - T_i)} \arg\left(\frac{R(T_i)}{R(T_{i+1})} \right) \tag{3.b}$$

$$\hat{w} = \frac{\lambda}{2\pi(n-1)} \sum_{i=1}^{n-1} \frac{1}{\sqrt{2(T_{i+1}^2 - T_i^2)}} \left[\ln \left| \frac{R(T_i)}{R(T_{i+1})} \right| \right]^{1/2}, \tag{3.c}$$

where the overall maximum unambiguous velocity is

$$v_a = \frac{\lambda}{4 \max(T_{i+1} - T_i)} \quad ; \quad i = 1, ..., n\text{-}1. \tag{4}$$

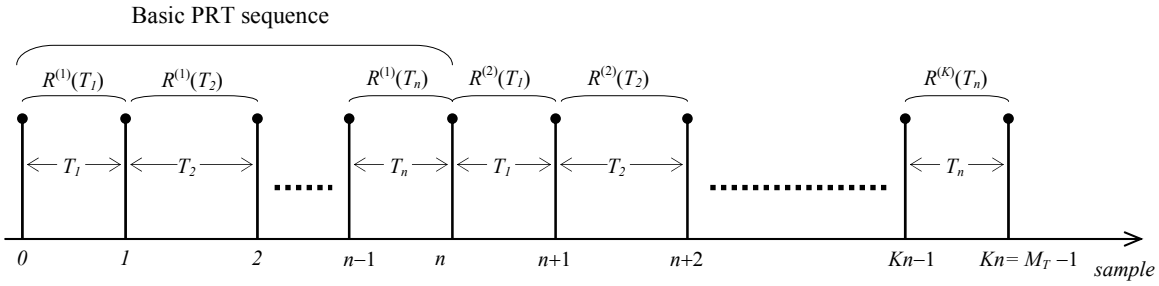

Fig. 1 Non-uniform samples in the multiple PRT scheme. The basic PRT scheme (one period) is repeated K times to get a total of M_T non-uniformly spaced samples. As shown in equation (2), estimates for the lag-1 autocorrelation for each PRT are obtained by considering the corresponding set of samples indicated with a superscript index $^{(k)}$.

Observe that for the case of n=2 (staggered PRT), the previous formulas reduce to the ones derived by Zrnic and Mahapatra (1985). In addition, note that velocities higher than this maximum unambiguous velocity can be measured by considering a reduced set of lag-1 autocorrelations in the set $\{R(T_i)\}$. Thus, it is also possible to estimate v and σ_v by using Eq. (3.b) and (3.c) when not all the $R(T_i)$'s are included in the averages.

The simulation of signal samples like the ones shown in Fig. 1 can be accomplished by using M_S uniformly sampled points and then "dropping" the unwanted samples to get the specified PRT scheme. Figure 2 illustrates this process for the simple case of T_1=1 ms and T_2=1.5 ms. Here we used a uniform sampling frequency ($1/T_s$) of 2 kHz and kept only the samples 0, 2, 5, 7, 10, 12, 15, ...

By using the previous formulas and simulation technique, the statistical performance of the modified pulse pair algorithm [i.e. Eqs. (3.b) and (3.c)] was evaluated and compared with the uniform-PRT pulse-pair algorithm. The results are shown in Fig. 3 for the staggered PRT case (n=2). In this example T_1=1 ms and T_2=1.5 ms, yielding a ratio T_1/T_2 = 2/3 and an unambiguous velocity of 50 m s^{-1} for a radar wavelength λ=0.1 m. To compute the statistics (i.e. mean and standard error) of both the mean velocity and the spectrum width estimators, 256 realizations of pure weather data time series were simulated, each with M_T = 64 pulses. The results in Fig. 3 agree with the ones presented by Zrnic and Mahapatra (1985).

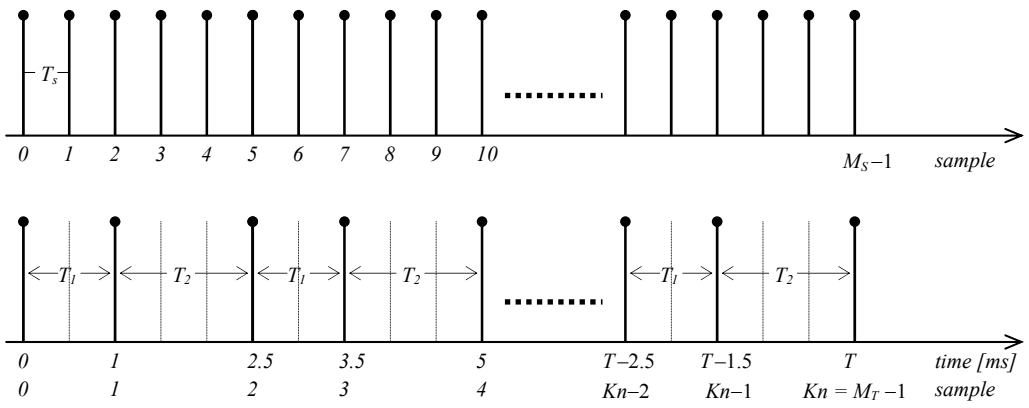

Fig. 2 Generation of signal samples with variable PRT. T_s = 0.5 ms, T_1 = 1 ms and T_2 = 1.5 ms.

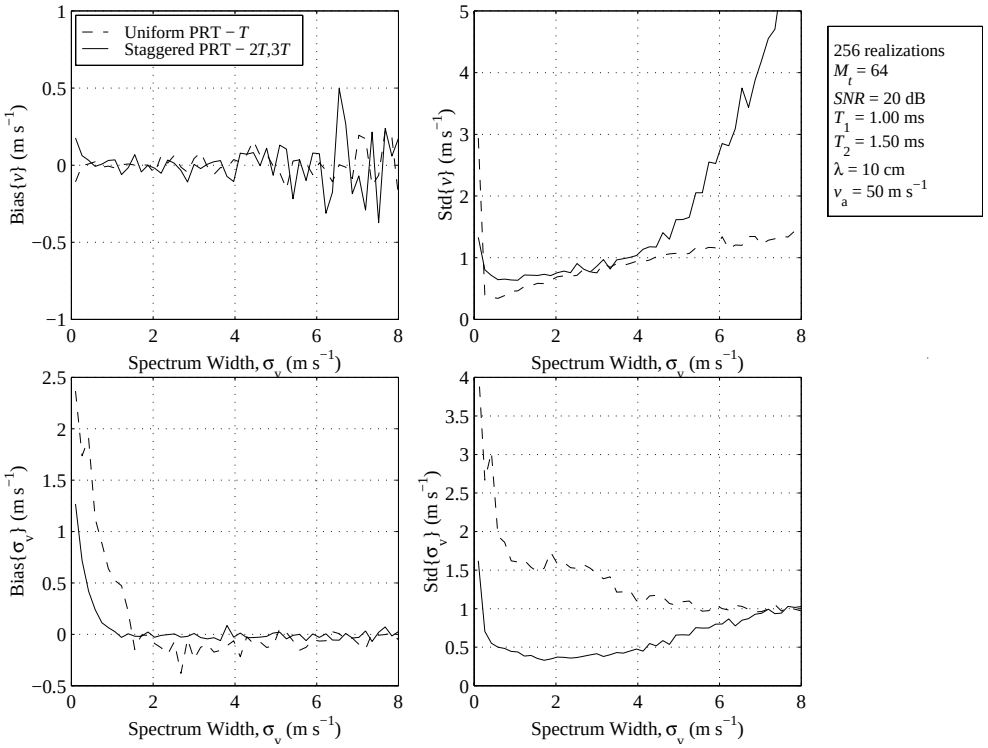

Fig. 3 Statistical performance of the pulse pair algorithm. Staggered PRT with T_1=1 ms, T_2=1.5 ms and M_T= 64 pulses. Uniform PRT with T_s=T_2−T_1 for same unambiguous velocity and M_S= 160 pulses for same dwell time. For both schemes 256 realizations of time series data were simulated with λ=10 cm and *SNR*=20 dB.

4. Ground Clutter Filter

As stated previously, ground clutter filters (GCF) are high-pass filters that ideally remove a few frequency components at either side of the zero Doppler velocity and leave the rest of the spectrum almost intact. It is very important to comply with this property during the design phase, because any changes in the magnitude response will directly bias the estimates of the three parameters of interest. On the other hand, it is relatively easy to prove that the phase characteristic of the filter is immaterial. To observe this, recall that power, mean velocity and spectrum width estimates depend on the estimated autocorrelation function of the filtered weather signal. It is well known that the power spectral density (*psd*) of the output of a linear time-invariant filter $S_y(\omega)$ is related to the

psd of the input $S_x(\omega)$ by the magnitude square of the frequency response of the filter. That is

$$S_y(\omega) = S_x(\omega)\left|H(\omega)\right|^2 . \tag{5}$$

Moreover, the autocorrelation function is uniquely determined by the corresponding *psd* through a Fourier transform pair relation. Because the phase response of the filter is not involved in this transformations it has no effect on the autocorrelation.

Unfortunately, this analysis does not apply when sampling is non-uniform. The linear time-invariant filter theory becomes useless when dealing with input samples arriving at different rates. Intrinsically, the non-uniform sampling process introduces a new series of complications in the analysis and design of suitable filters for clutter suppression. Nevertheless, a few approaches have been studied for clutter rejection filters operating with samples at non-uniform rates.

Banjanin and Zrnic (1991) used a time-varying filter that alternates between two sets of coefficients, one for each of the staggered PRTs. Their filter was affected by the staggering process in such a way that distortions in magnitude and phase occurred at frequencies given by integer multiples of $1/(T_1+T_2)$. A complicated, yet questionable scheme was proposed to mitigate the deleterious effects at these frequencies. On the other hand, Chornoboy (1994) proposed a multiple PRT scheme where the effects of non-uniform spacing would be spread uniformly over the unambiguous velocity interval. This might lead to tolerable degradation of velocity estimates everywhere. However, no comprehensive simulations or analysis of Chornoboy's filter are available.

Here we investigate the suitability of regression filters for ground clutter elimination and compare performance to the 5^{th}-order elliptic infinite-impulse-response (IIR) ground clutter filter (GCF) implemented in the WSR-88D. Application of regression filters to clutter suppression in Doppler ultrasonic blood flow meters was presented by Hoeks *et al* (1991) and extended by Kadi *et al* (1995) and Torp (1997) in the context of uniform PRT. Application of first order regression GCF to wind profiling radars is demonstrated by May and Strauch (1998). As a further step, we attempt to

extend practical application of regression filters to Doppler weather radars that use variable PRTs, and analyze some of the inherent problems discussed above.

4.1. Orthogonal Polynomials

The essential element of a regression filter is the operation that projects the input signal into what we identify as the "clutter signal subspace." This projection block performs the approximation of the input signal using a linear combination of the functions in the basis representing the subspace of interest. Consequently, the filter designer faces the issue of defining the functions in the basis of such subspace according to the filter performance specifications.

Projections of elements from a vector space S (the signal vector space) into a subspace W of S (the clutter signal space) can be efficiently performed when this subspace is represented by an orthogonal basis B. However, orthogonality alone is not sufficient to completely specify this basis. To improve the computational efficiency of this filtering process, we can limit the functions in B to polynomials over a set of discrete points on the real line. Therefore, for the general case, B will be a set of discrete orthonormal polynomials over a non-uniformly spaced set of sampling times.

Orthogonal polynomials have received a lot of attention in applications such as rational interpolation, least squares polynomial approximation, and smoothing of non-linear functions. Egecioglu and Koc (1992) presented an efficient algorithm to generate this set of polynomials over an arbitrary set of points $\{t_m\} = \{t_0, t_1, \cdots, t_{M_T-1}\}$. In their work they consider the generation of a basis $B = \{b_0(t), b_1(t), \ldots, b_p(t)\}$ [1] where for every $i \neq j$, $0 \leq i, j \leq p$

$$\left(b_i(t), b_j(t)\right) = \sum_{m=0}^{M_T-1} b_i(t_m) b_j(t_m) = 0 . \qquad (6)$$

[1] t is included to explicitly show that each element of B is a function of time

This set of orthogonal polynomials can be generated using the classical three-term recursion formula

$$b_{i+1}(t_m) = (t_m - \alpha_i) b_i(t_m) - \beta_i b_{i-1}(t_m) \quad \text{for } 0 \le i \le p \text{ and } 0 \le m \le M_T - 1, \tag{7}$$

with $b_{-1}(t_m) = 0$ and $b_0(t_m) = 1$, and where α_i and β_i are constants determined as

$$\alpha_i = \frac{\left(t b_i(t), b_i(t)\right)}{\left(b_i(t), b_i(t)\right)}, \; \beta_i = \frac{\left(b_i(t), b_i(t)\right)}{\left(b_{i-1}(t), b_{i-1}(t)\right)}. \tag{8}$$

For p=5 the set of orthogonal polynomials is depicted in Figure 4 over a sample set given by $\{t_m\}$={0, 2, 5, 7, 10, 12, 15, ... , 77}, i.e. M_T=32 with staggered PRT and underlying time set corresponding to T_1/T_2=2/3.

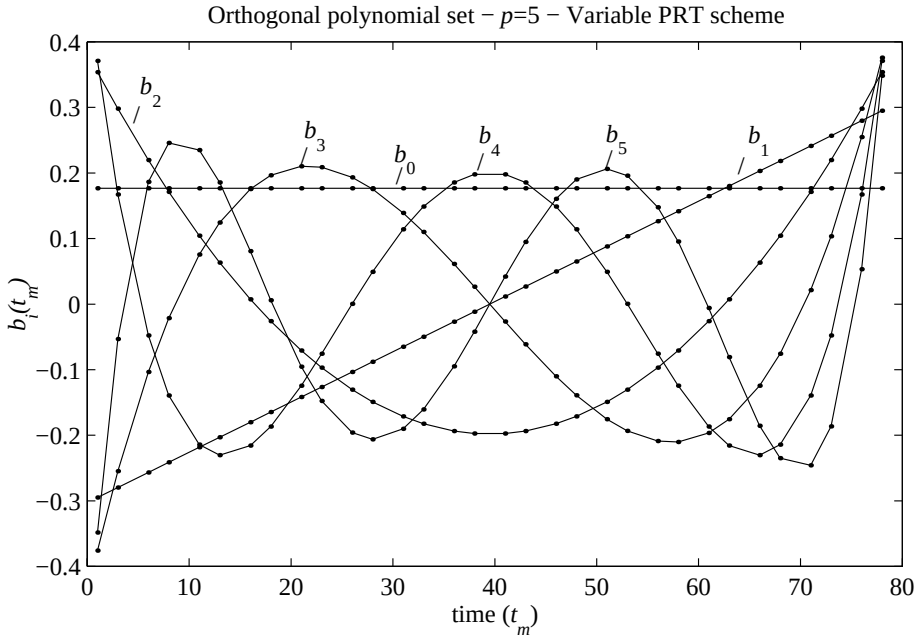

Fig. 4 Orthogonal polynomials on a non-uniformly spaced time grid with T_1/T_2=2/3.

4.2. Regression Filters

Classical digital filters can be divided into two classes: finite impulse response (FIR) and infinite impulse response (IIR) filters. For either class, filtering is achieved by

superposition of signal samples. Unlike these filters, regression filters approximate their input signals with polynomial functions in the time domain, and their design is not based on traditional tools such as the impulse or frequency responses. In our case, it can be assumed that the clutter signal varies slowly compared to the weather echo signal, and consequently can be approximated by a polynomial of a relatively low degree. This approximation is usually performed using least-squares methods or the equivalent transformation which projects the input signal samples $V(t)$, $t \in \{t_m\}$ onto the subspace W spanned by a basis B consisting of p+1 orthonormal polynomials. This set of polynomials is given by $B=\{b_0(t),b_1(t),b_2(t),...,b_p(t)\}$, where each $b_i(t)$ ($0 \le i \le p$) is a polynomial of i^{th} degree. That is, $b_i(t) = c_{0i} + c_{1i}t + ... + c_{ii}t^i$ with $t \in \{t_m\}$. Then, the projection $\hat{V}(t)$ (i.e. the clutter signal) is obtained by constructing a linear combination of the elements of the basis B, i.e. implication is that $\hat{V}(t)$ is in W and therefore

$$\hat{V}(t_m) = \sum_{i=0}^{p} \alpha_i b_i(t_m). \tag{9}$$

Accordingly, the residue $V_f(t_m) = V(t_m) - \hat{V}(t_m)$ is associated with the portion of the input signal that is not contained in the clutter subspace W [i.e. it is orthogonal to $\hat{V}(t)$]. The coefficients α_i 's are computed using the classical formula (Papoulis 1986, 146-154)

$$\alpha_i = \frac{(\mathbf{V}, \mathbf{b_i})}{\|\mathbf{b_i}\|^2} = \frac{\sum_{m=0}^{M_f-1} V(t_m) b_i(t_m)}{\sum_{m=0}^{M_f-1} b_i^2(t_m)} \qquad i = 0, 1, ..., p. \tag{10}$$

Generalization in this analysis is not lost if each element of B is normalized such that $\|\mathbf{b_i}\| = 1$, where $\|\mathbf{b_i}\|^2 = (\mathbf{b_i}, \mathbf{b_i})$. In addition, to simplify the notation define the basis matrix **B** and the coefficient vector **A** as

$$\mathbf{B} = \begin{bmatrix} b_0(t_0) & b_0(t_1) & \cdots & b_0(t_{M_f-1}) \\ b_1(t_0) & b_1(t_1) & \cdots & b_1(t_{M_f-1}) \\ \vdots & \vdots & \ddots & \vdots \\ b_p(t_0) & b_p(t_1) & \cdots & b_p(t_{M_f-1}) \end{bmatrix} \text{ and } \mathbf{A} = \begin{bmatrix} \alpha_0 \\ \alpha_1 \\ \vdots \\ \alpha_p \end{bmatrix}. \tag{11}$$

Then, assuming a normalized base, Eqs. (9) and (10) can be rewritten as $\hat{\mathbf{V}} = \mathbf{B}^{\mathbf{T}}\mathbf{A}$. Substitution of $\mathbf{A} = \mathbf{B}\mathbf{V}$ produces $\hat{\mathbf{V}} = \mathbf{B}^{\mathbf{T}}\mathbf{B}\mathbf{V}$ and the residue or filtered signal $\mathbf{V_f}$ can be expressed as

$$\mathbf{V_f} = \mathbf{V} - \hat{\mathbf{V}} = (\mathbf{I} - \mathbf{B}^{\mathbf{T}}\mathbf{B})\mathbf{V}, \tag{12}$$

where the regression filter matrix is defined by

$$\boxed{\mathbf{F} = \mathbf{I} - \mathbf{B}^{\mathbf{T}}\mathbf{B}}. \tag{13}$$

The regression filter block diagram is shown in Fig. 5 and from Eq. (12) it is apparent that the filter is linear (as matrix multiplication is a linear transformation), time-varying, and responds to the general input-output equation of the form

$$y(t_l) = \sum_{m=0}^{M_f-1} f(t_l, t_m)x(t_m) \;; \quad l = 0, ..., M_f - 1, \tag{14}$$

where $f(t_l,t_m)$ are the entries of the matrix **F** defined in Eq. (13).

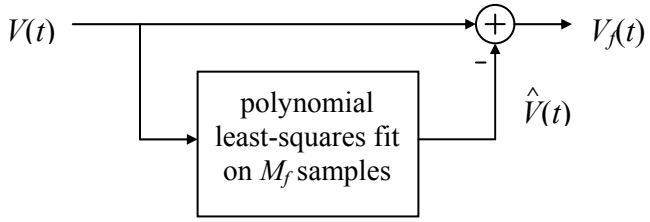

Fig. 5 Regression filter block diagram. Signals are processed in independent segments or blocks of M_f samples each. In any case, M_f need not be equal to the total number of samples M_T in the input signal used to estimate spectral moments.

The filter matrix **F** depends only on p and M_f, so it can be pre-computed for real-time applications and does not need to be recomputed if the notch width or sampling scheme do not change. In any case, M_f need not be equal to the total number of samples M_T in the input signal used to estimate spectral moments.

Several approaches can be devised if $M_T > M_f$, according to the way the input signal is decomposed into the samples blocks to be least squares fitted. For our study, we adopted overlapping blocks, attempting to simulate the behavior of a moving average filter. In this implementation, special care must be taken on both ends of the input sequence. The scheme can be summarized as follows: the first $M_f/2$ output samples are computed as in Eq (14). From sample $M_f/2 + 1$ and up to sample $M_T - M_f/2$ the output is computed by sliding the $(M_f/2 + 1)$-th column of **F**, i.e. t_l inside the summation in Eq(14) is fixed to $M_f/2+1$. Finally, the last $M_f/2$ output samples are computed as in Eq (14). Note that if $M_T = M_f$, the process reduces to Eq. (14).

4.3. Frequency Response of the Regression Filter

The frequency response $H(\omega)$ of a linear shift-invariant system can be defined as the change in magnitude and phase of a complex exponential signal $e^{j\omega t}$ which is passed through the system. More precisely, let $x(t)$ and $y(t)$ be the input and output of the filter whose impulse response is given by $h(t)$. Let $x(t) = e^{j\omega_0 t}$, then the output $y(t)$ can be obtained by convolving $x(t)$ with $h(t)$, i.e.

$$\begin{aligned} y(t) = h(t) * x(t) = \sum_{t' \in \{t_m\}} h(t')x(t-t') = \sum_{t' \in \{t_m\}} h(t')e^{j\omega_0(t-t')} = \\ = \left(\sum_{t' \in \{t_m\}} h(t')e^{-j\omega_0 t'} \right) e^{j\omega_0 t} = H(\omega_0)x(t), \end{aligned} \tag{15}$$

in which $H(\omega_0)$ describes the frequency response at $\omega = \omega_0$.

As previously stated, the regression filter is time varying. However, the output to a given signal of M_f samples is always the same regardless when this block of M_f samples is encountered in the filtering process. We will exploit this fact in deriving an expression

for the frequency response of the regression filter using Eq. (14) in an analogous fashion as Eq. (15). That is, consider the regression filter whose input is an exponential of the form $e^{j\omega t}$. The output of this filter is

$$y(t_l) = \sum_{m=0}^{M_f-1} f(t_l, t_m) e^{j\omega t_m} \quad ; \; l = 1, ..., M_f \tag{16}$$

$$y(t_l) = \sum_{m=0}^{M_f-1} f(t_l, t_m) e^{j\omega(t_m - t_l)} e^{j\omega t_l} = \left(\sum_{m=0}^{M_f-1} f(t_l, t_m) e^{j\omega t_m} \right) e^{-j\omega t_l} x(t_l) . \tag{17}$$

Then, by noting the form of (17) we define

$$H(\omega, t_l) = F_l(-\omega) e^{-j\omega t_l} , \tag{18}$$

where $F_l(\omega) = \sum_{m=0}^{M_f-1} f(t_l, t_m) e^{-j\omega t_m}$ is the DFT of $f(t_l,t_m)$ with constant parameter l. Finally, accounting for all the values of l in the M_f-sample segment

$$H(\omega) = \tfrac{1}{M_f} \sum_{l=0}^{M_f-1} F_l(-\omega) e^{-j\omega t_l} . \tag{19}$$

Using the results of Eq. (13), each entry in **F** is given by

$$f(t_l, t_m) = \delta(t_l - t_m) - \sum_{i=0}^{p} b_i(t_l) b_i(t_m) , \tag{20}$$

where $\delta(t)$ is the usual discrete-time impulse sequence. Then

$$F_l(\omega) = e^{-j\omega t_l} - \sum_{i=0}^{p} b_i(t_l) B_i(\omega) , \tag{21}$$

where $B_i(\omega)$ is the DFT of $b_i(t)$. Then,

$$H(\omega) = 1 - \tfrac{1}{M_f} \sum_{i=0}^{p} B_i(-\omega) \left[\sum_{l=0}^{M_f-1} b_i(t_l) e^{-j\omega t_l} \right] , \tag{22}$$

and finally the frequency response of the regression filter is given by

$$\boxed{H(\omega) = 1 - \tfrac{1}{M_f} \sum_{i=0}^{p} \left| B_i(\omega) \right|^2}. \qquad (23)$$

Note that because $H(\omega)$ is real, the phase response of this filter is constant and we only need to consider the changes in the magnitude response. Also, as depicted in Fig. 5, $H(\omega)$ consists of a direct path, the "1" in Eq. (23), and a weighted path given by the least squares fit projection and corresponding to the second term in the same equation.

The frequency response of the regression filter depends on the number p of elements in B (i.e. the maximum degree of the polynomials used for approximation) and on the number of samples M_f in each processing block. High-frequency signals exhibit rapid changes in time and hence, they are better approximated as p increases. Therefore, by increasing p, we allow high-frequency components to be subtracted from the input signal, and this results in a broader notch width. On the other hand, for a fixed p higher frequencies are eliminated if the filter window M_f is shorter. That is, polynomials of a relatively low degree can still "follow" high-frequency components. Consequently, the notch width of the regression filter increases when M_f decreases. This dependence is illustrated in Fig. 6 for the uniform PRT scheme. From these plots, we can confirm that the notch bandwidth increases with p and decreases as M_f increases. Observe that in Fig. 6.c $M_T = 2M_f$ and the filtering scheme discussed in the previous section is implemented. Frequency responses for the regression filter change just slightly with respect to Fig. 6.b.

The WSR-88D 5th-order elliptic GCF can be programmed for three different suppression levels: low suppression, medium suppression, or high suppression. These selections correspond to notch widths of 2.36 m s^{-1} (±1.18 m s^{-1}), 3.12 m s^{-1} (±1.56 m s^{-1}), and 5.06 m s^{-1} (±2.53 m s^{-1}), which do not change with the number of samples M_T. The steady-state frequency responses of the low, medium and high suppression 5th-order elliptic GCF for the WSR-88D are also plotted for comparison. The general form of the transfer function of this filter is

$$H_{WSR-88D}(z) = \frac{b_0 + b_1 z^{-1} + b_2 z^{-2} + b_3 z^{-3} + b_4 z^{-4} + b_5 z^{-5}}{1 - a_1 z^{-1} - a_2 z^{-2} - a_3 z^{-3} - a_4 z^{-4} - a_5 z^{-5}}, \tag{24}$$

where the coefficients a_i's and b_i's are obtained from the classical design formulas for digital elliptic filters as given in Parks and Burrus (1987).

During scans at elevation larger than 1.5° the WSR-88D transmits an interlaced waveform whereby a batch of low PRTs is for Doppler measurements. Therefore, to achieve the indicated frequency response, the GCF uses a two-pulse extension of the *step initialization* process, as described by Sirmans (1992). This process consists of setting the filter memories to steady state, assuming a d.c. clutter signal with amplitude equal to the first pulse in the batch. For this analysis, we adopt the number of samples $M_T = 32$ in the input signal. An increase in the number of samples forms a sharper notch, which tends to the theoretical steady-state response of (24). In the WSR-88D, the actual number of samples in a radial depends on the volume coverage pattern (VCP) mode, and can be from 33 to 111 samples. Therefore, the adopted $M_T = 32$ represents a worst-case scenario.

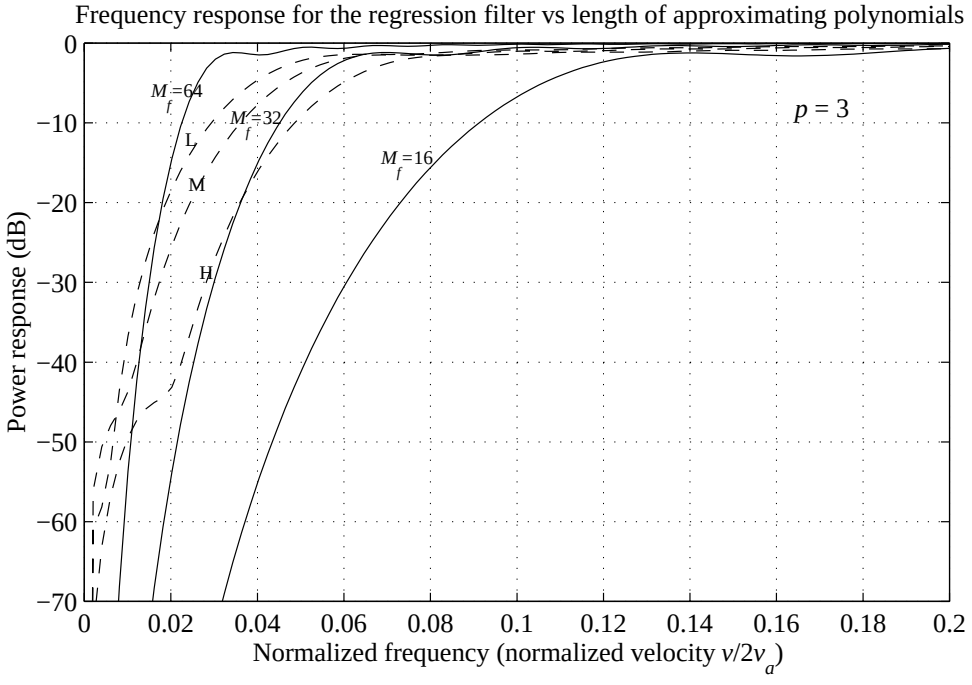

(a)

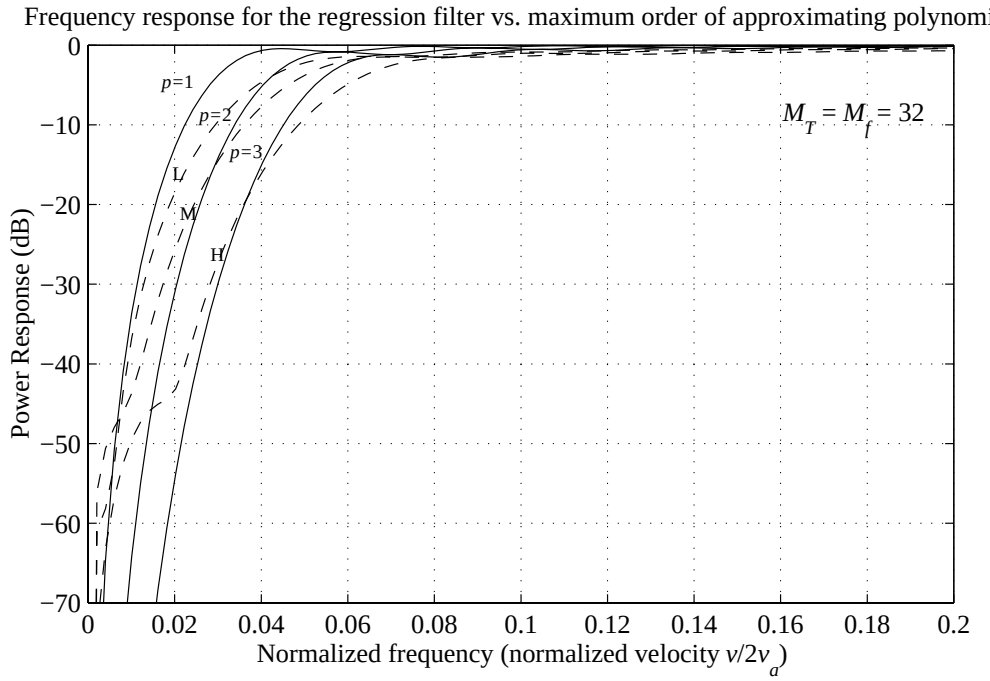

(b)

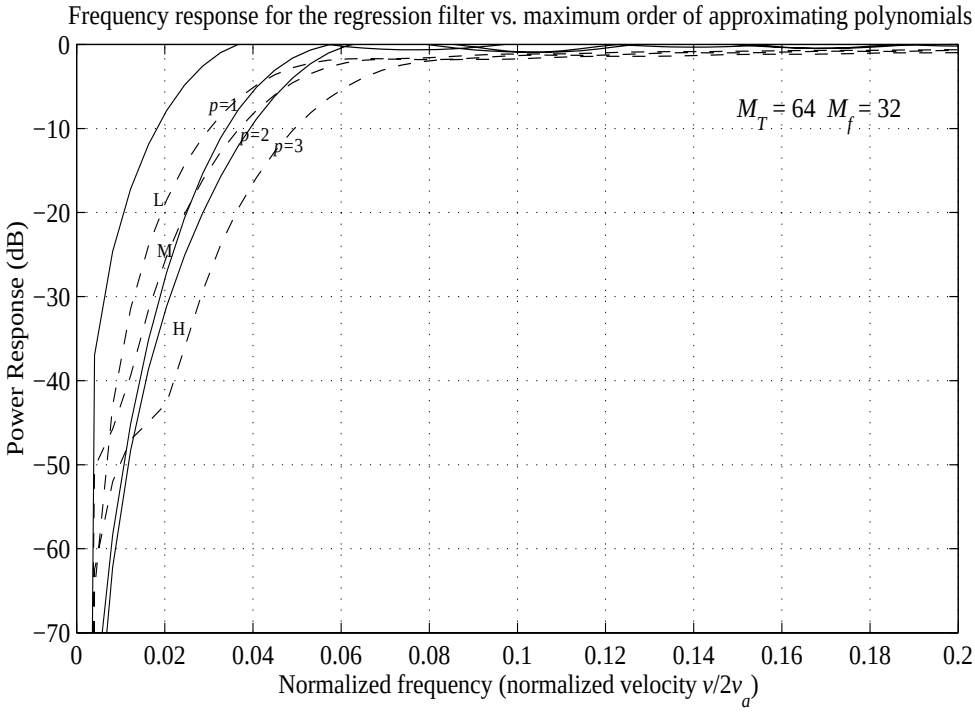

(c)

Fig. 6 Regression filter frequency response with p and M_f as parameters. The frequency responses of the low (L), medium (M) and high (H) suppression 5th-order elliptic filter used in the WSR-88D are also included for comparison. The two-pulse extension of the step initialization process is used to improve the response, i.e. suppress the transient due to the step inputs at the beginning of pulse bursts for velocity estimation.

Figure 7 shows how the filter's 3 dB notch width depends on the number of samples, for both classes of GCFs. As a useful tool for further comparison, we find a direct equivalence between each suppression level of the 5th-order elliptic filter and the order of approximating polynomials in the regression filter. We observe, for instance, that for $p = 3$ and $M_f = 32$, the notch width of the regression filter closely matches that of the medium suppression GCF in the WSR-88D.

The regression filter has several attractive properties compared to the GCF currently implemented in the WSR-88D. While the latter is greatly influenced by the filter's transient response characteristics, the regression filter inherently avoids these transients (i.e. these filters do not cause transients). Moreover, regression filters design methods diverge from the ones used with classical filters, because their implementation consists of a matrix multiplication instead of a set of equations to evaluate recursively for each time. Thus, the regression filter is well suited for modern array processors.

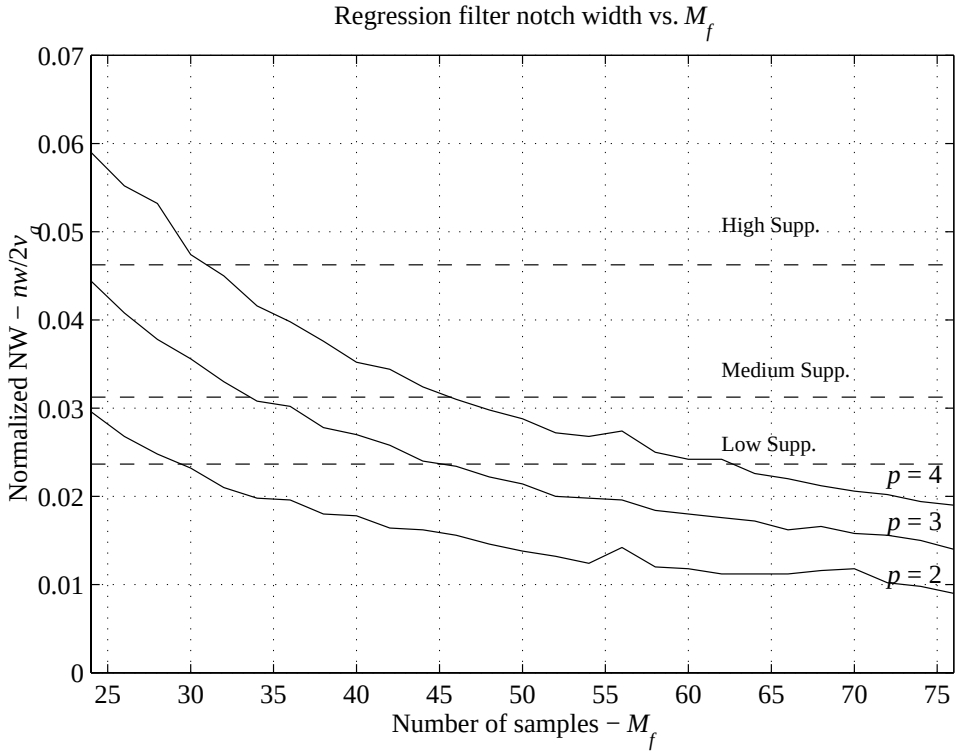

Fig. 7 Regression filter notch width vs. number of uniformly spaced samples and order of approximating polynomials.

5. Performance Analysis of the Regression Filter

5.1. Uniform PRT Scheme

In this section, we carry simulations to establish the performance of the regression filter and compare it with the 5th-order elliptic GCF implemented in the WSR-88D. The clutter signal is modeled as a narrow-band Gaussian process with zero mean velocity. This clutter and white noise are added to a synthetic weather signal (Zrnic 1975). Then, the composite signal is filtered to remove the ground clutter and finally the first three moments of the weather Doppler spectrum are estimated with the classical pulse pair algorithm. This process is shown in Fig. 8.

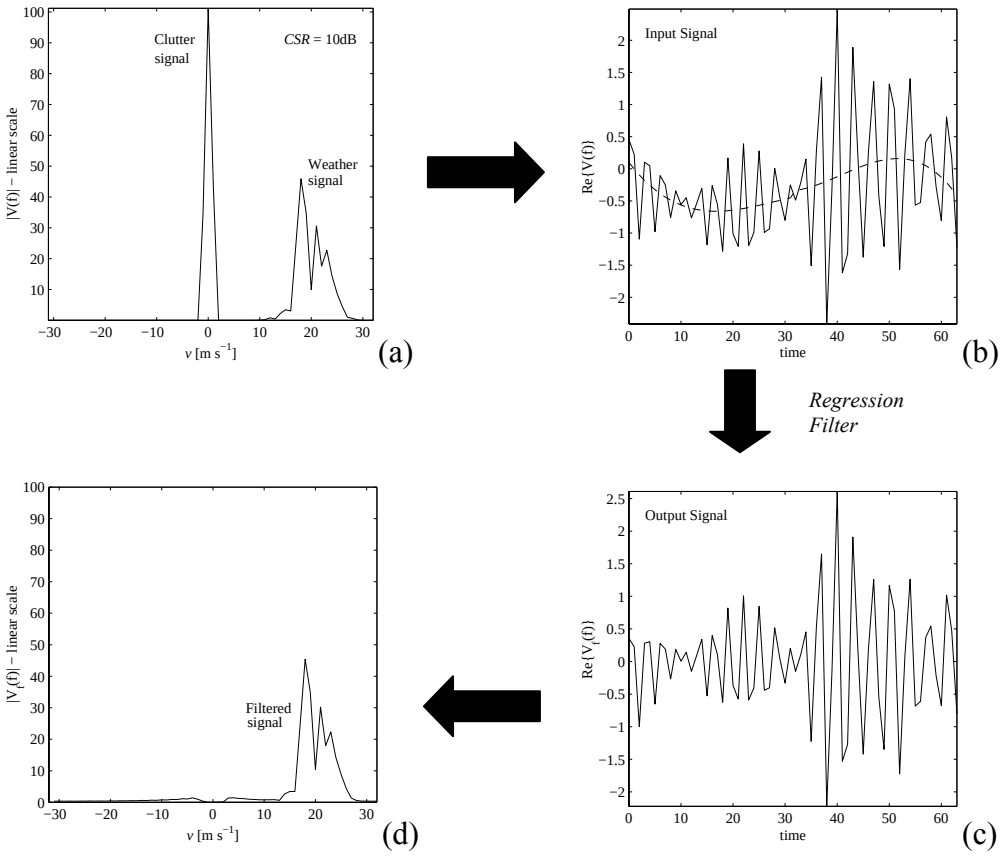

Fig. 8 Clutter filtering process using a regression filter. (a) Spectrum of a weather signal contaminated with ground clutter. (b) Time-domain representation of the composite signal. The dashed line is the 3rd-order polynomial fit to this signal, i.e., the estimated clutter. (c) Filtered signal in the time domain used to determine S, v and σ_v from Eq. (3). (d) Spectrum of the filtered signal.

Two parameters of interest for these simulations are: the signal-to-noise ratio (*SNR*) and the clutter-to-signal ratio (*CSR*) which are defined as $SNR(dB) = 10\log_{10}(S/N)$ and $CSR(dB) = 10\log_{10}(C/S)$ where *S*, *C* and *N* are signal, clutter and noise powers respectively. The clutter filter suppression ratio (*CFSR*), a measure of the filter's performance, is defined by $CFSR(dB) = 10\log_{10}(P_{out}/P_{in})$. In this equation P_{in} and P_{out} are the powers measured at the input and output of the clutter filter respectively (note that $P_{in} = C+S+N$ and ideally $P_{out} = S+N$). Figure 9 shows the *CFSR* if no weather signal is present at the input of the filter with the clutter spectrum width as a parameter. The behavior of both the regression filter and the WSR-88D elliptic filter described in Section 4 is depicted in the same figure. It is observed that for the most common case of narrow clutter spectrum widths, i.e. $\sigma_c < 0.5$ m s^{-1}, the suppression ratio of the regression filter with $p = 4$ is at least 10 dB better than the one achieved by the high-suppression elliptic GCF. In general, the regression filter performs better than the comparable elliptic filter, especially if the spectrum width of the clutter is narrow.

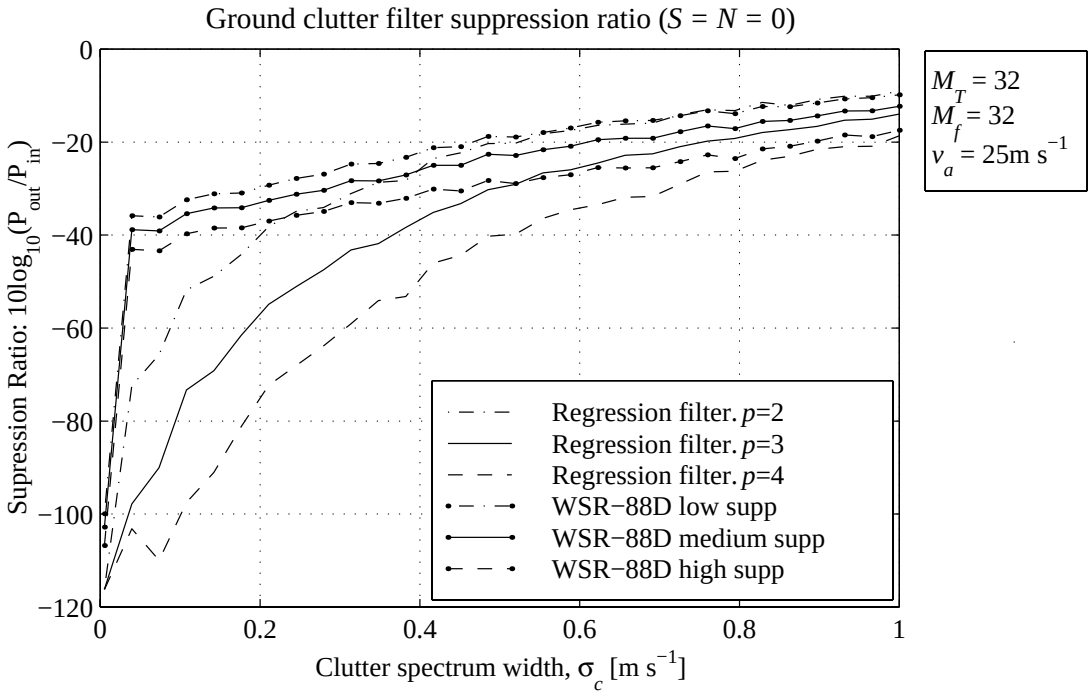

Fig. 9 Suppression ratio vs. clutter signal spectrum width when no weather signal is present.

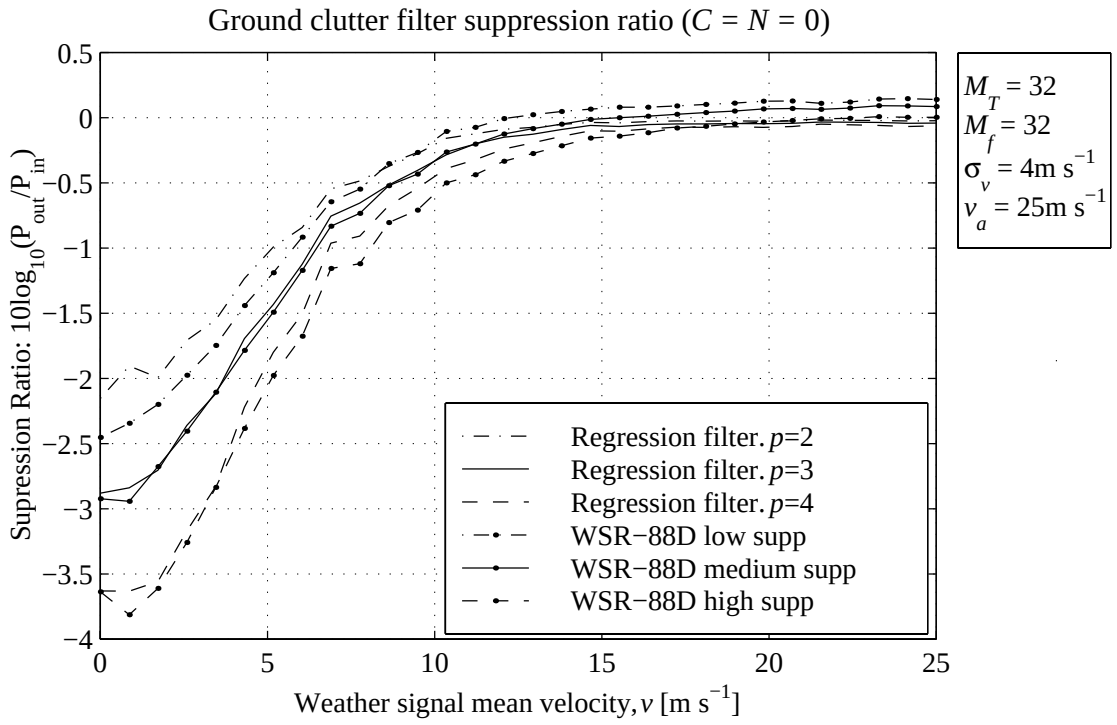

(a)

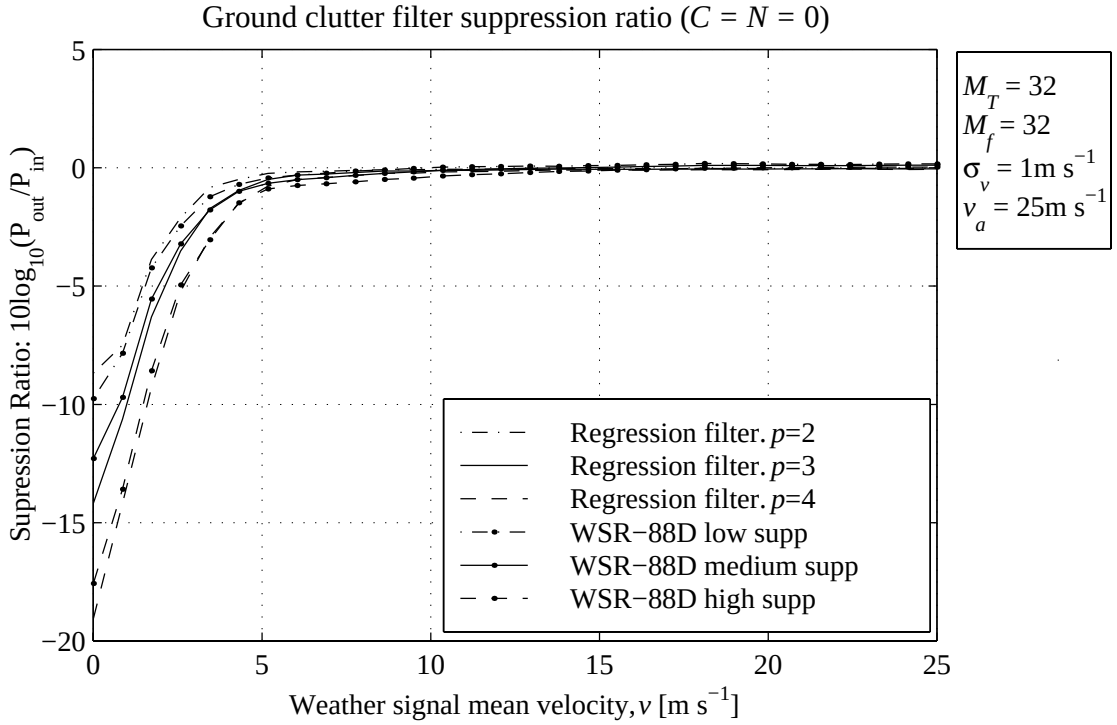

(b)

Fig. 10 Suppression ratio vs. signal spectrum mean velocity when no clutter signal is present. (a) σ_v = 4 m s^{-1} (median value in severe storms) ; (b) σ_v = 1 m s^{-1} (typical value in stratiform rain)

The suppression of weather-like signals by these filters is plotted in Fig. 10, where the mean velocity changes from 0 to 25 m s^{-1}, and the spectrum width is set constant. A value of 4 m s^{-1} in Fig. 10.a simulates the median found in severe storm observations (Doviak and Zrnic, 1993). Over 1 dB of suppression is observed for signal mean velocities below 5 to 8 m s^{-1}, depending on the notch width of the filter. At that, performances of regression filters are comparable to the elliptic filters of corresponding notch width. Similar results hold for weather signals with spectrum width of 1 m s^{-1} (typical of stratiform rain) except the 1 dB suppression is for velocities below 3.5 to 4.5 m s^{-1} (Fig. 10.b). These curves indicate the power estimation biases one can expect if the mean velocity of the weather signal is close to zero. However, when the mean velocity of the weather signal is well away from 0 m s^{-1}, neither of the filters biases the power estimates.

For a more realistic situation, a weather signal was combined with the ground clutter and the ratio P_{out}/S was computed for different *CSR*s. This analysis is shown in Figs. 11.a and 11.b for a *CSR* of 20 and 40 dB respectively. The clutter spectrum width is set at 0.28 m s^{-1} for the first case (Fig 11.a) and 0.23 m s^{-1} for the second case (Fig. 11.b). The first value is the same as the one used for testing the WSR-88D ground clutter filter performance (Sirmans, 1992). Measurements on the WSR-88D in Norman, OK indicate that the mean of clutter spectrum width is 0.25 m s^{-1}; therefore, 0.28 m s^{-1} is in the worst case category. However, this value is too large if the *CSR* equals 40 dB causing excessive contamination, and a smaller value of 0.23 m s^{-1} is adopted in Fig. 11.b. It is seen in Fig. 11 that the reflectivity estimates can have a significant negative bias if the mean Doppler velocity of the weather signal is such that its spectrum overlaps the one of the ground clutter. This is because the ground clutter filter also removes a portion of the weather signal. In addition, we observe a small positive bias (WSR-88D low suppression) if the mean Doppler velocity departs from the origin for a *CSR* of 20dB, because the clutter signal is not fully removed by the filter. For the *CSR* of 40dB, we found that the elliptic GCF does not remove the clutter signal completely leaving an almost constant bias along the entire velocity range. The same occurs with the 2^{nd}-order regression filter but the 3^{rd}- and 4^{th}-order regression filters had no bias. Evidently, this effect gets worse

for larger *CSR* and wider clutter spectrum width but it can be controlled by adjusting the ground clutter filter frequency response.

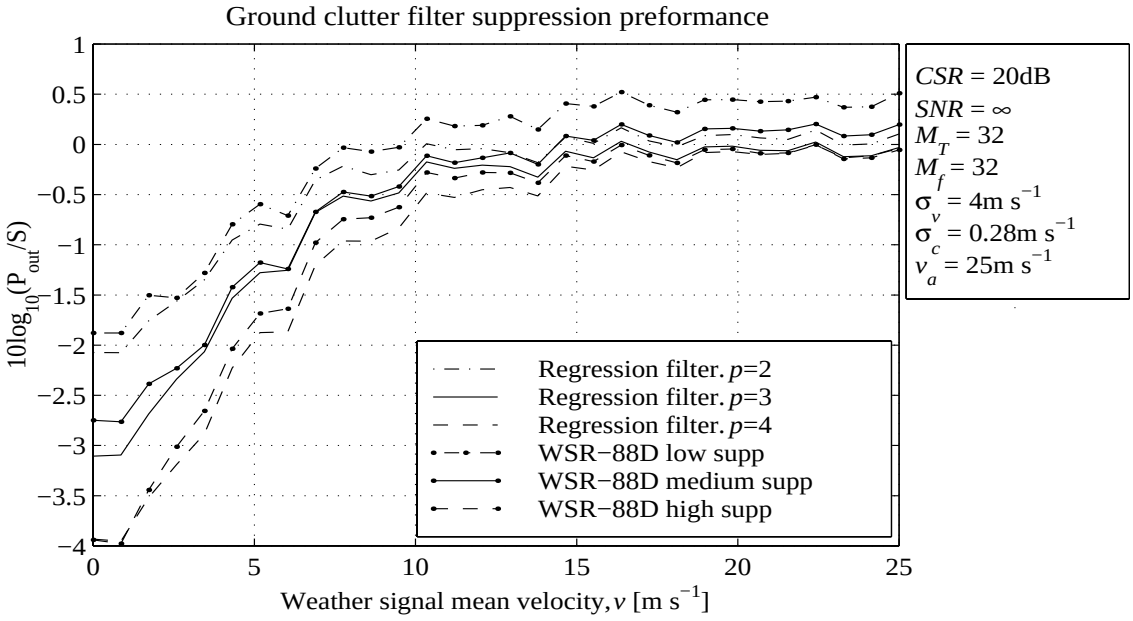

(a)

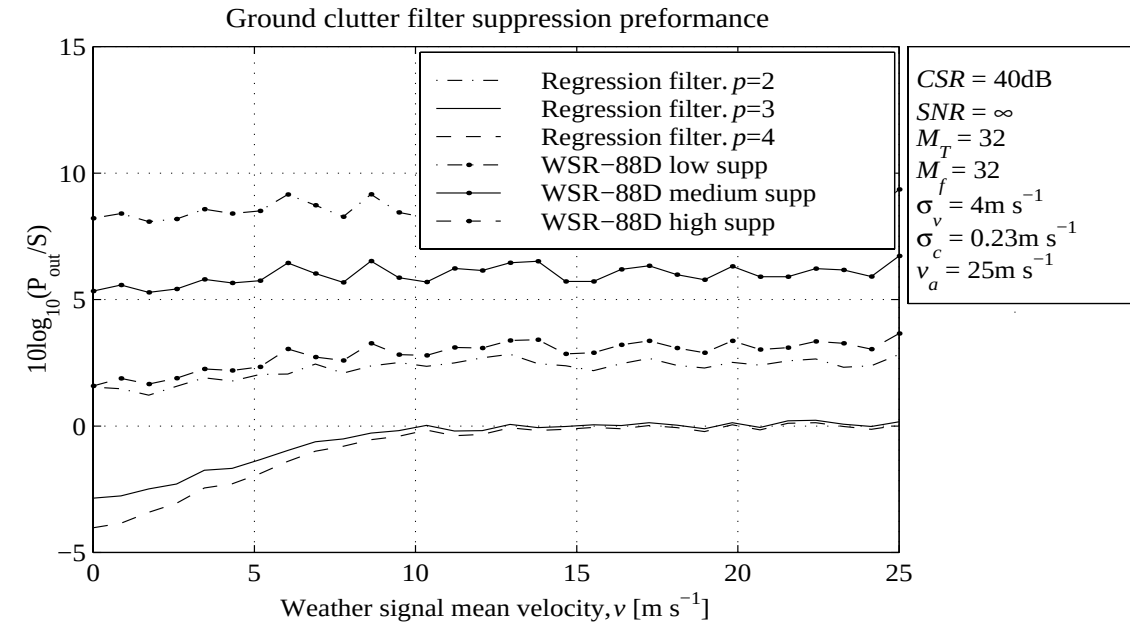

(b)

Fig. 11 Supp. ratio of regression and elliptic GCFs vs. weather signal mean velocity. (a)*CSR*=20dB, (b)*CSR*=40dB

As the ultimate goal is to accurately recover the three first spectral moments of the weather signal, the pulse pair statistical performance for different *CSR*s was computed vs. (a) the weather signal mean velocity and (b) the weather signal spectrum width for both regression and elliptic WSR-88D filters. The results are shown in Fig. 12.

Consider first the case when the weather signal mean velocity is a parameter and the spectrum width is randomly selected from the interval (2,6) m s^{-1} (Figs. 12.a and 12.b). Here we observe that there are large positive biases for both the mean velocity and the spectrum width estimates when the true mean velocity of the weather signal is less than approximately 5 m s^{-1}. As explained before, this is due to overlap of the weather and clutter spectra. A part of this spectrum close to zero velocity is eliminated by the filter; therefore, the non-filtered components bias the velocity upward. Mean velocity bias for the regression filter is about 0.25 m s^{-1} larger than for the elliptic filter at $v < 10$ m s^{-1}. The standard deviation for the velocity estimation remains under 2 m s^{-1} and very close to the performance of the pulse-pair algorithm in the absence of clutter. Keeping a high *SNR* and increasing the *CSR*, from Fig. 12.a to Fig. 12.b, does not significantly affect the statistical performance of the pulse pair algorithm. When increasing the order of the regression filter, from p=3 to p=4 (not shown), we do observe an increase in the biases for weather signals with mean velocities near 0 m s^{-1} which is caused by the broader notch width of this filter.

Next, we use the weather-signal spectrum width as a parameter and randomly select its mean velocity from the interval (-25,25) m s^{-1} (Figs. 12.c and 12.d). In this case, we notice that the variation in mean velocity bias and standard deviation increase with the weather signal spectrum width. This effect is consistent with the autocovariance algorithm performance; it is and slightly more evident if there is contamination by the clutter signal. The bias in v and the standard deviations for the two filters are comparable. A slightly smaller bias and standard deviation are seen in spectrum width estimates. Because the GCF does not remove the clutter signal completely, for small spectrum widths, we observe a positive bias in the spectrum width estimates, which increases with the *CSR*. From all these figures, we conclude that influences of the regression filter and

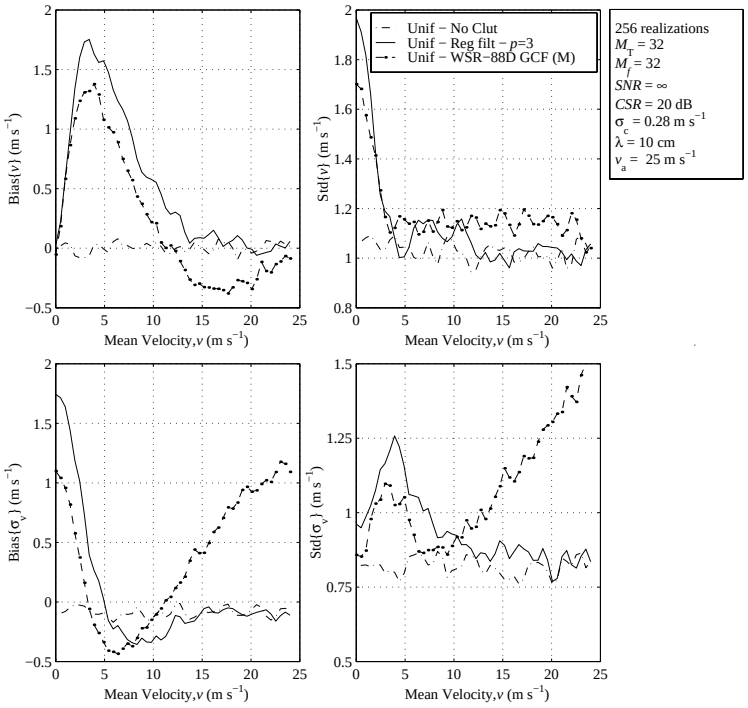
Unif − No Clut
Unif − Reg filt − p=3
Unif − WSR−88D GCF (M)
256 realizations
M_T = 32
M_f = 32
SNR = ∞
CSR = 20 dB
σ_c = 0.28 m s^−1
λ = 10 cm
v_a = 25 m s^−1
Bias{v} (m s^−1)
Std{v} (m s^−1)
Bias{σ_v} (m s^−1)
Std{σ_v} (m s^−1)
Mean Velocity, v (m s^−1)

(a)

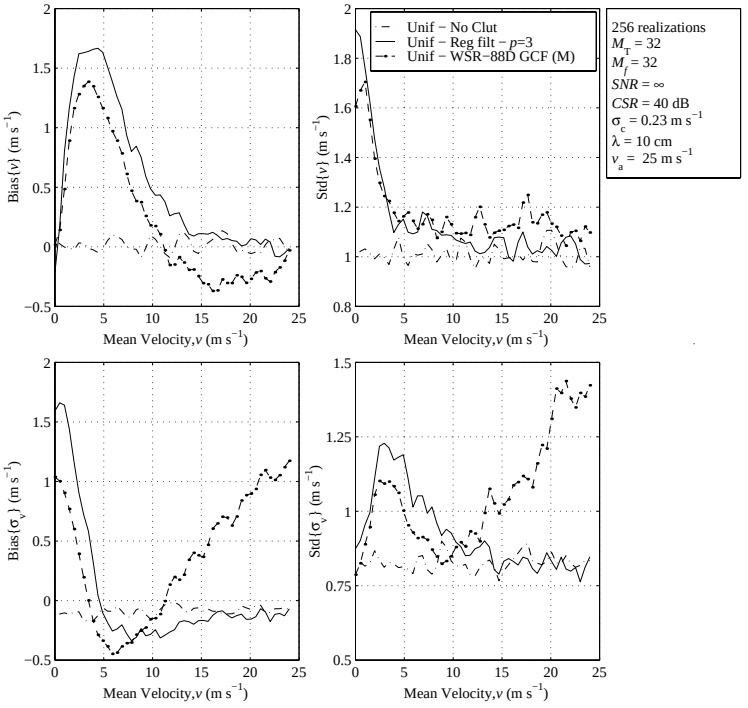
Unif − No Clut
Unif − Reg filt − p=3
Unif − WSR−88D GCF (M)
256 realizations
M_T = 32
M_f = 32
SNR = ∞
CSR = 40 dB
σ_c = 0.23 m s^−1
λ = 10 cm
v_a = 25 m s^−1
Bias{v} (m s^−1)
Std{v} (m s^−1)
Bias{σ_v} (m s^−1)
Std{σ_v} (m s^−1)
Mean Velocity, v (m s^−1)

(b)

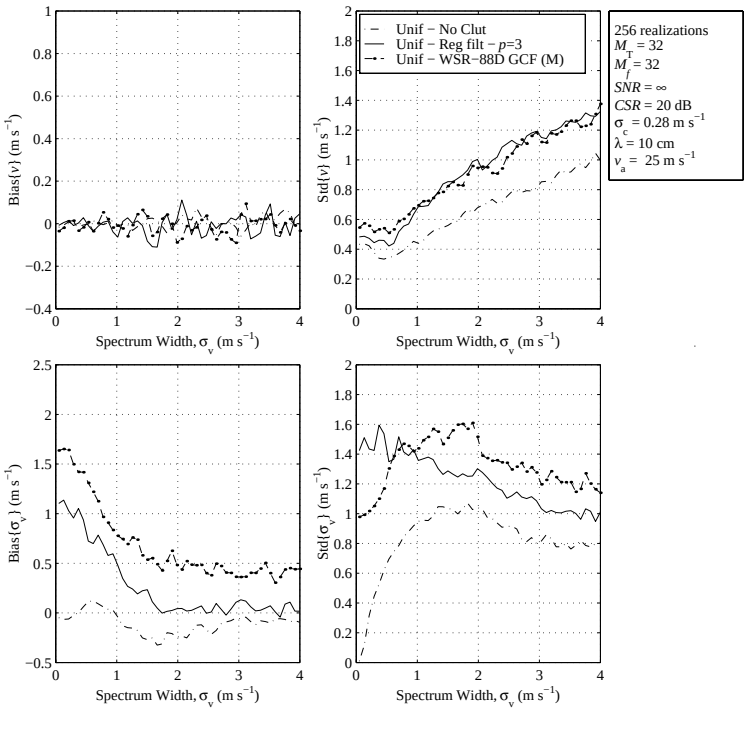

(c)

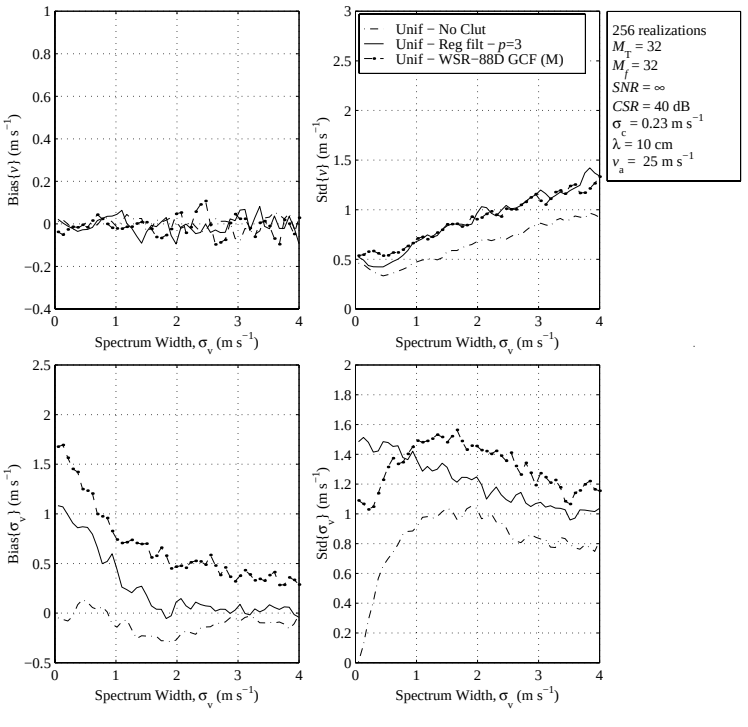

(d)

Fig. 12 Pulse pair algorithm statistical performance. (a),(b) vs. the weather signal mean velocity; (c),(d) vs. the weather signal spectrum width. For all simulations we used a medium-suppression filter (p = 3), 256 realizations, and an unambiguous velocity of 25 m s^{-1}.

the corresponding elliptic filter on the statistical performance of pulse pair estimators are comparable.

5.2. Application of filters to the WSR-88D data

Time series data have been collected with a WSR-88D in Memphis at the lowest elevation of 0.5° while the antenna was scanning at 12° s^{-1}. Sixty-four samples of the in-phase component (Fig. 13.a) reveal a slowly varying clutter signal and possibly weak weather signal. The Doppler spectrum (Fig. 13.b) has a peak at zero, which is 75 dB above the receiver noise level. This large spectral dynamic range has been routinely observed on both Memphis and Norman WSR-88D and testifies to the very high quality of the system. The spectrum width of this ground clutter is 0.23 m s^{-1}, the *CSR* is 33 dB and the *SNR* is 26 dB.

Application of the regression filter with p=3 produces signals in Fig. 14 whereas the medium suppression elliptic filter provides the signals in Figs. 15 and 16. The regression filter with M_f =32 is applied to the 64 input samples similarly to a moving average filter as explained in Section 4.2. Note how the in-phase signal after regression filtering has no discernible slow varying component whereas after filtering with the elliptic filter it does. This is also reflected in the spectral shapes at and close to zero velocity. The clutter spectrum has been suppressed at least 40 dB below the weather peak after application of the regression filter (Fig. 14.b) and it is slightly below the weather peak after application of the elliptic filter (Fig. 15.b). For the non-initialized elliptic filter in Fig. 16, the results are inferior, as evidenced by the higher residual clutter power with spectral peaks slightly above the weather signal peak level. This demonstrates the advantage of step initialization in the WSR-88D.

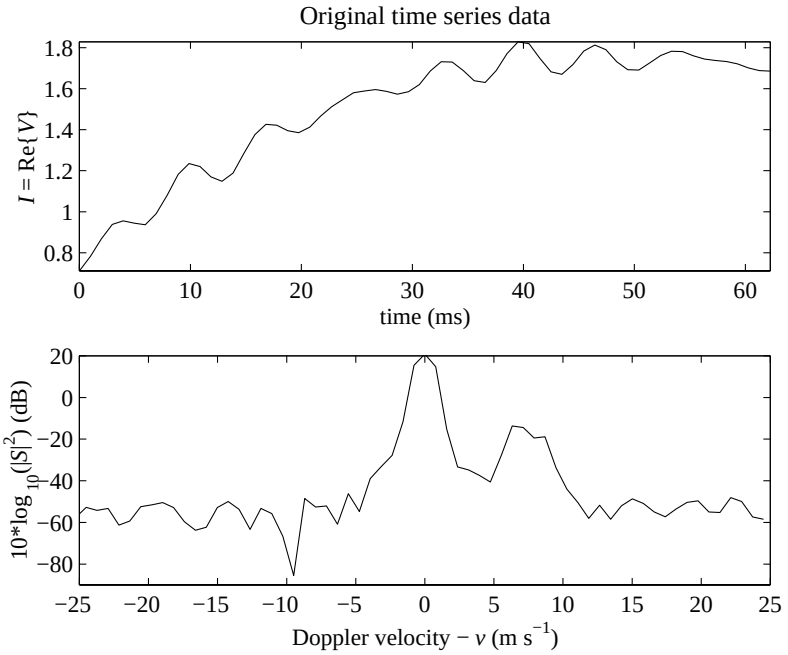

Fig. 13 Data collected with the WSR-88D in Memphis at a range of 15 km. (a) In-phase component and (b) Doppler spectrum of the time series to which the von Hann window has been applied.

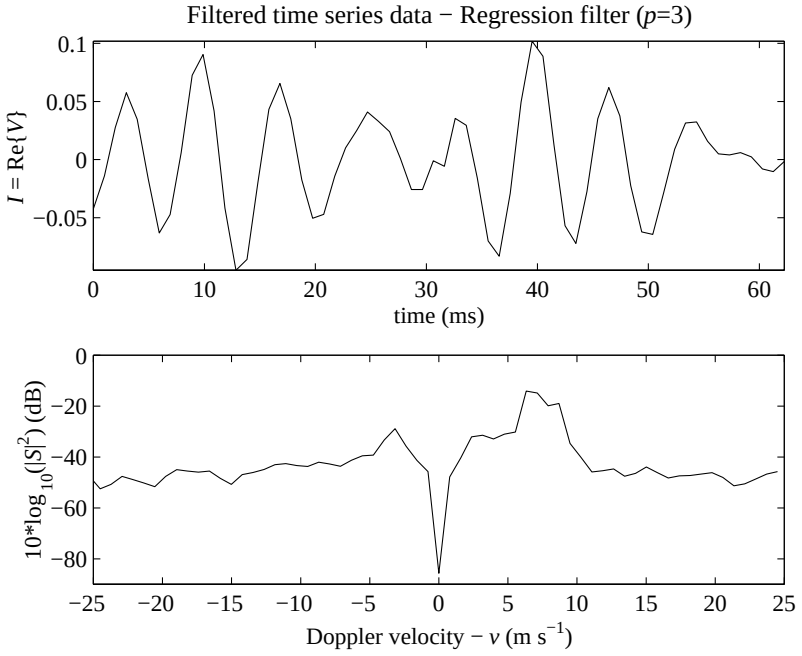

Fig. 14 Time series data filtered with the "medium suppression" regression filter (p=3). (a) In-phase filtered component and (b) Doppler spectrum of the filtered signal (weighted with the von Hann window).

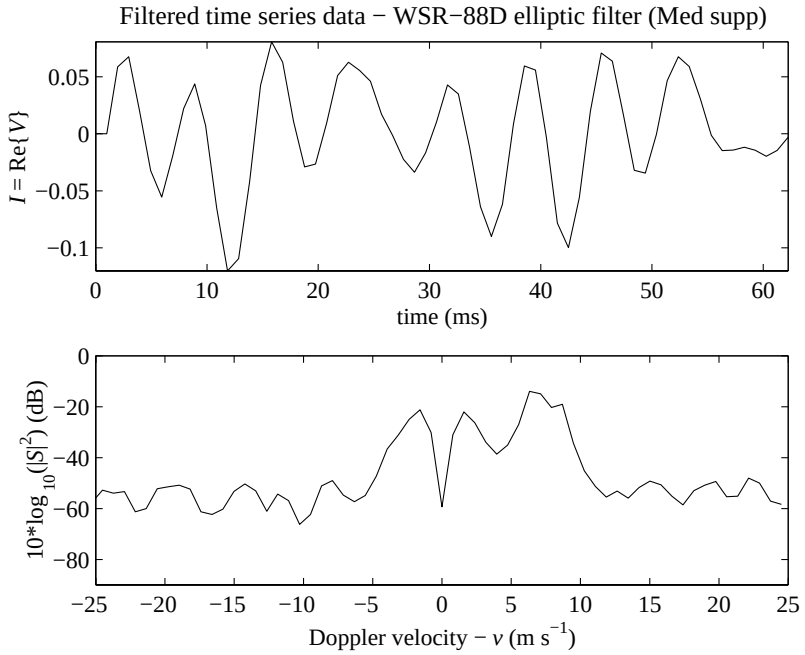

Fig. 15 Same as in Fig. 14 except the medium suppression WSR-88D ground clutter filter has been applied.

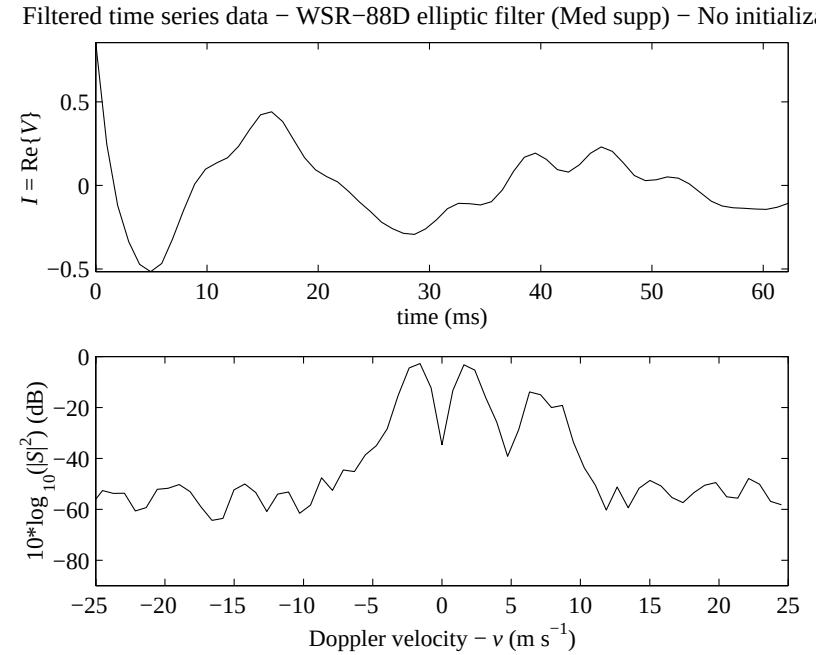

Fig. 16 Same as in Fig. 15 except the 5th-order elliptic ground clutter filter has *not* been initialized according the the two-pulse extension of the step initialization, as implemented in the WSR-88D.

5.3. Staggered PRT Scheme

As pointed out in the introduction, the motivation for this analysis is the need for an effective method to suppress ground clutter in variable PRT sequences used to mitigate the effects of range-velocity ambiguities. The regression filter appears to be a promising approach to solve this problem because it can be readily generalized to the non-uniform PRT scheme (as it does not require using frequency-domain design techniques). Moreover, the necessary tools exist for generating a set of orthogonal polynomials over a non-uniform sampling grid and consequently it is feasible to implement a ground clutter filter in the context of variable PRT. However, as demonstrated by simulations, the regression filter does not avoid the previously encountered problems (Banjanin and Zrnic, 1991). This filter also exhibits additional notches at the normalized frequencies given by $f = nT_S/(T_1+T_2)$, where $n \in Z$ and T_S is the corresponding underlying uniform PRT from which the staggered PRT signal is derived.

Throughout these simulations, we used the staggered PRT scheme with different stagger ratios T_1/T_2. Figures 17 and 18 show the suppression ratio computed using the parameters as in Figs. 9 and 10. From these plots, we observe that the clutter suppression is comparable to the one achieved by the same filters on a uniform sequence of pulses. However, this is not sufficient to accept the regression filter as a good candidate for ground clutter canceling. The regression filter frequency response is deficient. Plots for the two values of T_1/T_2 (Fig. 19) reveal the undesirable notches. The first plot (Fig 19.a) corresponds to T_1/T_2=2/3 and clearly exhibits additional notches located at $f = 0.2\ n$. The second plot (Fig. 19.b) corresponds to T_1/T_2=3/4 and shows notches at $f = 0.1429\ n$, where as before $n \in Z$. As found by Banjanin and Zrnic (1991), these additional notches introduce phase non-linearities which ultimately deteriorate the performance of the pulse pair algorithm (because the algorithm is based on the phase of the autocorrelation of the weather signal). This fact was verified by evaluating the statistical performance of the autocovariance algorithm (Doviak and Zrnic, 1993, eq. 7.6a) on this particular PRT scheme for T_1/T_2=2/3. The results are presented in Fig. 20 where we can see large bias and standard deviation located exactly at the additional notch frequencies.

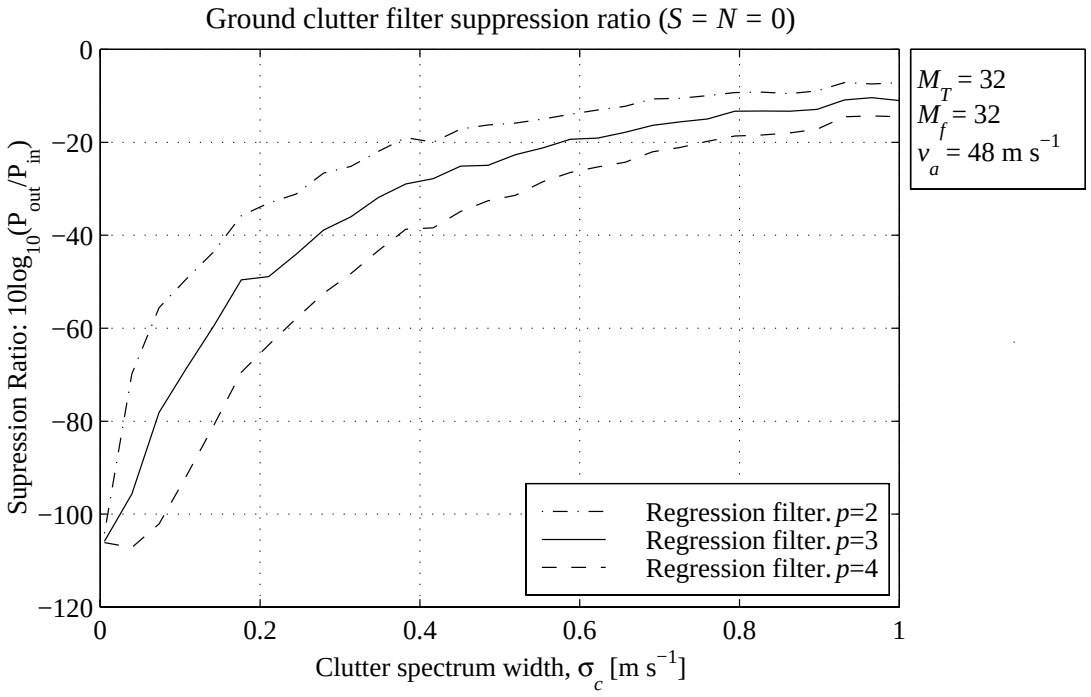

Fig. 17 Suppression ratio vs. clutter signal spectrum width (no weather signal is present). Staggered PRT scheme with T_1/T_2=2/3.

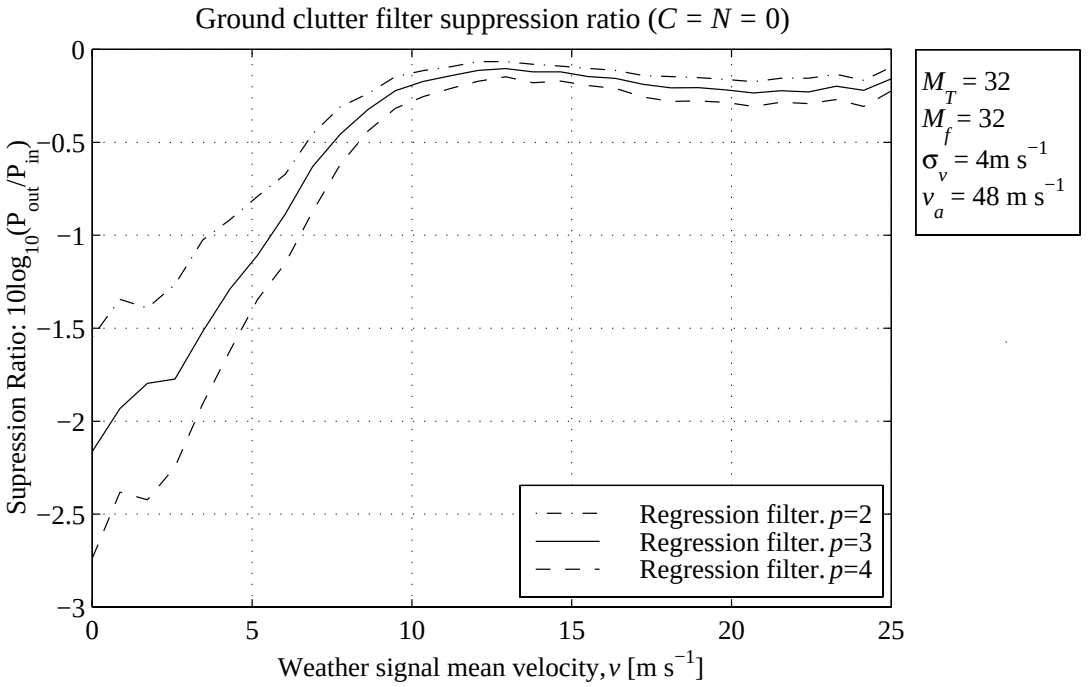

(a)

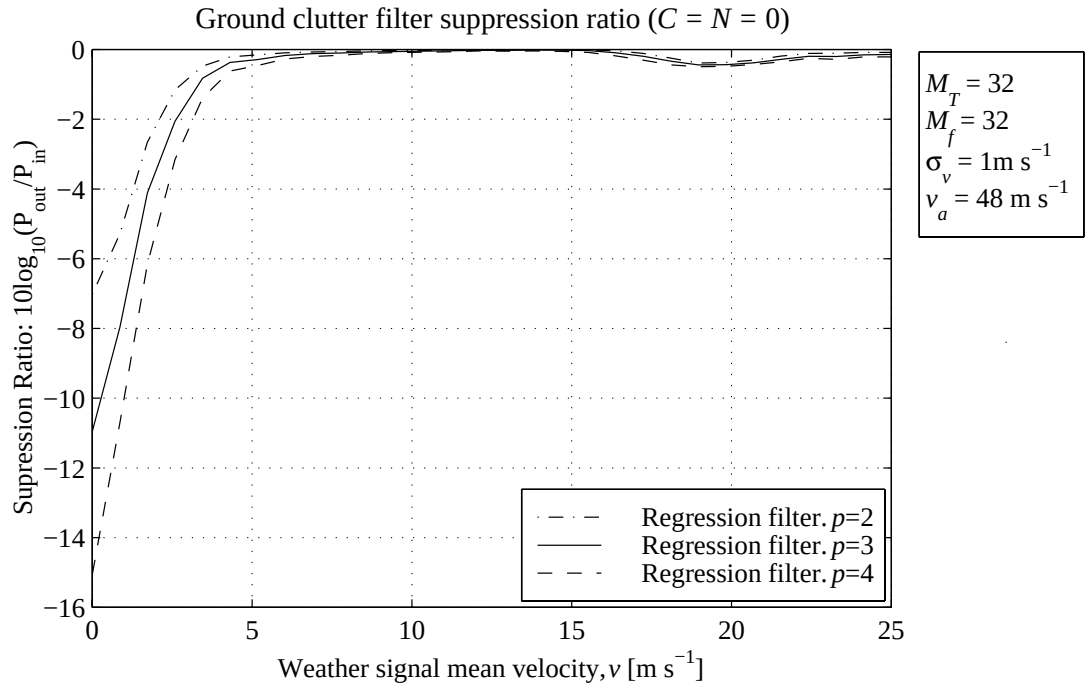

(b)

Fig. 18 Suppression ratio vs. weather signal mean velocity (no clutter signal is present). Staggered PRT scheme with T_1/T_2=2/3.

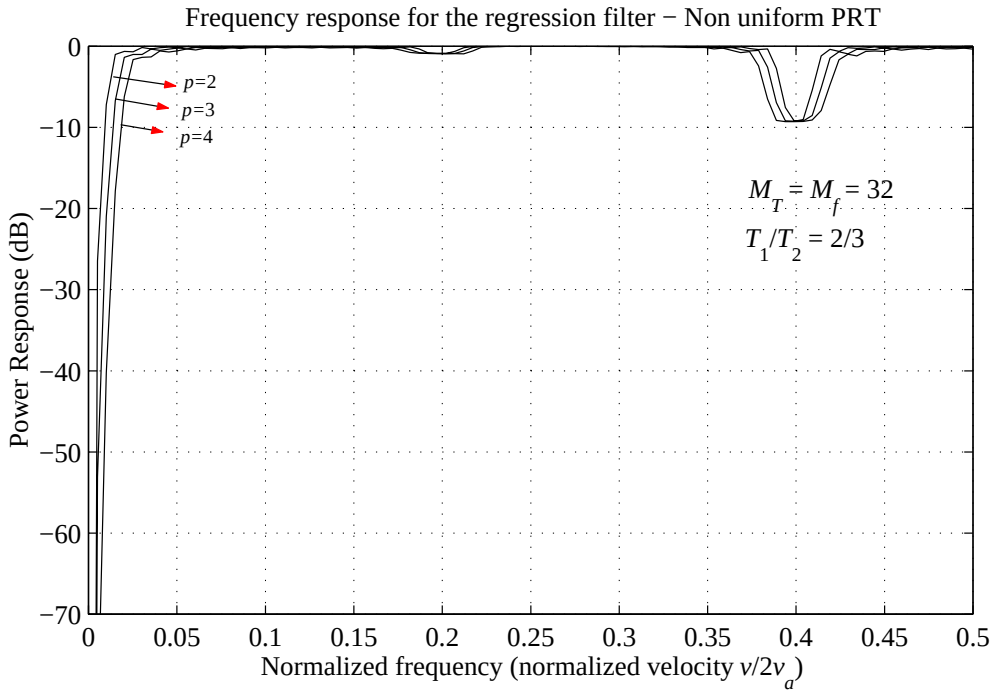

(a)

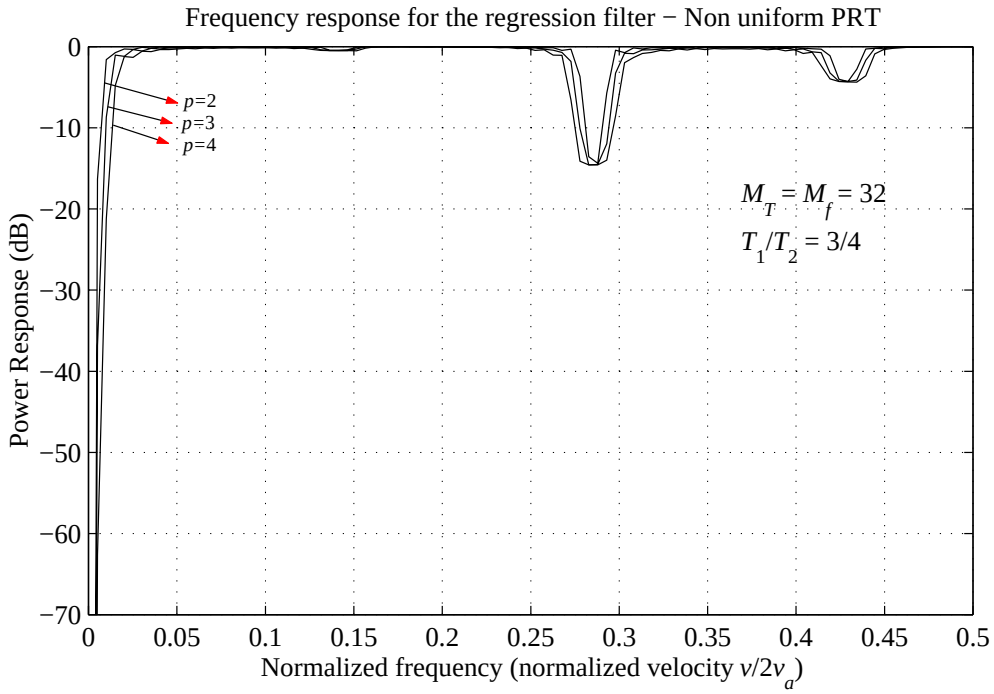

(b)

Fig. 19 Frequency response of a regression filter applied to a staggered PRT sequence.

(a) T_1/T_2=2/3, (b) T_1/T_2=3/4

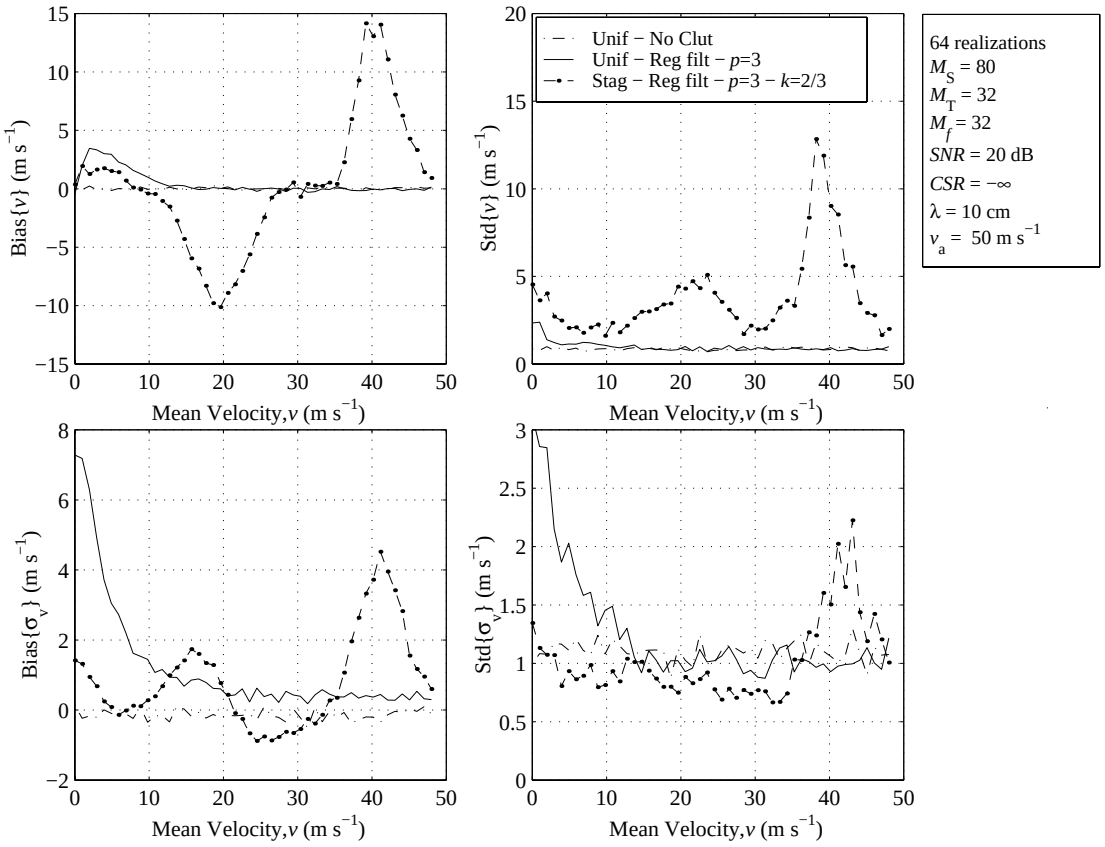

Fig. 20 Statistical performance of the autocovariance algorithm applied to a staggered PRT sequence (T_1/T_2=2/3). The performances on (1) a uniform PRT sequence with no ground clutter and (2) a uniform PRT sequence and a 3rd-order regression filter are also included. The uniform and staggered PRT sequences were generated such that dwell times are the same for both. In the uniform PRT sequences M_S=80, T_s=0.5 ms, and in the staggered PRT sequence M_T=32, T_1=2T_s, and T_2=3T_s; therefore, both yield a maximum unambiguous velocity v_a of 50 m s^{-1}. Large biases and standard deviations appear at and near integer multiples of $\lambda/[2(T_1+T_2)]$ (m s^{-1}) when the regression filter is applied to the signal with staggered samples.

6. Future Work

There are still some variations to the variable PRT techniques and other aspects of the design that deserve to be explored. These can be classified into the following approaches:

- Block PRT: where T_i is repeated m_i consecutive times in an attempt to emulate the uniform PRT scheme while keeping the advantages of having more than one PRT for

an extended velocity range. The regression filter (or any other GCF) can be applied to each uniform batch independently.

- Jittered PRT: where the periodicity of the sampling process is destroyed by using the sequence $\{T_1, T_2, T_1+\delta_1, T_2+\delta_1, \cdots, T_1+\delta_m, T_2+\delta_m\}$ where $\delta_m << T_1, T_2$. With this scheme, we expect the notches to be almost uniformly distributed along the entire range of frequencies (Doppler velocities).

- Almost Uniform PRT: where only one or two pulses with different PRT are added to the uniform PRT scheme. It is possible to get good velocity estimates from the uniform pulses, and then exploit information from pulses at different PRTs to correct velocity aliases by shifting the estimates to the actual Nyquist interval (adding integer multiples of $2v_a$). This scheme was proposed by Cornelius *et al* (1993).

- Extrapolation schemes as the one presented by Chornoboy (1993).

- Implementation of Eqs. 3.b and 3.c with different autocorrelation ratios to obtain better estimates of v and σ_v.

7. Conclusions

This initial report on regression filters tried to find the answer to two main questions: (1) will a regression filter perform better than the current 5th-order elliptic filter in the WSR-88D?, and (2) can this filter be applied to a non-uniform PRT sequence and if so, what are the consequences on spectral moment estimates?

First, we compared the performance of the regression filter scheme applied to a uniformly sampled sequence with that of the actual WSR-88D 5th-order elliptic filter. In the context of uniform PRT, regression filters present the advantage of easy implementation, not requiring filter initialization such as needed in the Doppler mode of data processing at higher than 1.5^o in elevation on the WSR-88D. Parameters that control the frequency response are the number of samples to which regression is applied and the degree of the regression polynomial. The increase in the polynomial degree (p) broadens

the filter's notch width because higher frequencies are subtracted from the signal. The notch width also broadens if the number of samples (M_f) decreases because then the regression polynomial replicates better high frequency components. Different families of approximating polynomials only affect the computational complexity of the implementation, which is considerably reduced when this set is orthonormal. Simulations indicate that the suppression characteristics of regression filters meet or exceed those of step-initialized IIR filters, in which transients degrade the theoretical frequency response. For p=3 and M_f=32, the regression filter approximates the performance of the medium-suppression 5th-order elliptic filter in the WSR-88D. Comparison of the two filters on an actual weather signal, collected by an operational WSR-88D, indicates that the regression filter performs better.

Next, we attempted to establish the feasibility of implementing this scheme for filtering clutter signals on a multiple PRT sequence. The answer to this second issue is not very promising at this time, but there are still many points to be explored, as briefly introduced in the previous section. The existing results, for the more difficult task of designing an effective clutter filter in the context of variable PRT, are not satisfactory. The regression filter in the staggered PRT scheme presents multiple notches at frequencies other than zero. This is a disadvantage because notches cause very large biases and standard deviation of the first three spectral moment estimates of the clutter-contaminated weather signals to which the filter is applied. In summary, two alternatives can be identified a) One is to come up with a design that neutralizes the spurious notches in the frequency response of the regression filter. b) The other is to try a different approach. It is possible that this problem could be handled effectively and efficiently by one of the schemes suggested for future investigation in the previous section.

8. References

Anderson, J.A., 1990: Evaluating ground clutter filters for weather radars*, Preprints, 20th Conf. Radar Meteor.*, Boston, MA, Amer. Meteor. Soc., 20A.

Banjanin, Z., and D. Zrnic, 1991: Clutter rejection for Doppler weather radars which use staggered pulses, *IEEE Trans. Geosci. Remote Sensing*, **29**, 4, 610-620.

Chornoboy, E.S., 1993: Clutter filter design for multiple-PRT signals, *Preprints, 26th Internat. Conf. on Radar Meteor.*, Norman, OK, Amer. Meteor. Soc., 235-237.

_____, and M.E. Weber, 1994: Variable-PRI processing for meteorologic Doppler radars, *Preprints, 1994 IEEE National Radar Conference*, Atlanta, GA, IEEE, 85-90.

Cornelius, R., R. Gagnon and F. Pratte, 1993: Data quality and ambiguity resolution in a Doppler radar system, United States Patent #5247303.

_____, _____ and _____, 1995: WSR-88D clutter processing and AP clutter mitigation, ERL/FSL NCAR/ATD NWS/OSF Report.

Doviak, R.J., and D. Zrnic, 1993: *Doppler Radar and Weather Observations*, 2nd ed. New York: Academic Press, 562 pp.

Egecioglu, O., and C. Koc, 1992: A parallel algorithm for generating discrete orthogonal polynomials, *Parallel Computing*, **18**, 649-659.

Heiss, W., D. McGrew, and D. Sirmans, 1990: NEXRAD: Next Generation Weather Radar (WSR-88D), *Microwave Journal*, **33**, 1, 79-98.

Hoeks, A.P., J.J. van-de-Vorst, A. Dabekaussen, P.J. Brands, and R.S. Reneman, 1991: An efficient algorithm to remove low frequency Doppler signals in digital Doppler systems, *Ultrason. Imag.,* **13**, 2, 135-44.

Kadi, A.P., and T. Loupas, 1995: On the performance of regression and step-initialized IIR clutter filters for color Doppler systems in diagnostic medial ultrasound, *IEEE Trans. Ultrason., Ferroelect., and Freq. Control*, **42**, 5, 927-937.

May, P.T., and R.G. Strauch, 1998: Reducing the effect of ground clutter on wind profiler velocity measurements, *J. Atmoss. Oceanic Technol.,* **12**, 4, 579-586.

Papoulis, A., 1986: *Signal Analysis*, 3rd ed. New York: McGraw-Hill, 431 pp.

Parks, T.W., and C.S. Burrus, 1987: *Digital Filter Design*, John Wiley & Sons, 342 pp.

Sirmans, D., 1992: Clutter filtering in the WSR-88D, NWS/OSF Report, Norman, OK.

_____, D. Zrnic, and B. Bumgarner, 1976: Extension of maximum unambiguous Doppler velocity by use of two sampling rates, *Preprints, 17th Conf. Radar Meteor.*, Seattle, WA, Amer. Meteor. Soc., 23-28.

Torp, H., 1997: Clutter rejection filters in color flow imaging: atheoretical approach, *IEEE Trans. Ultrason., Ferroelect., and Freq. Control*, **44**, 2, 417-424.

Weber, M.E., and E.S. Chornoboy, 1993: Coherent processing across multi-PRI waveforms, *Preprints, 26th Internat. Conf. on Radar Meteor.*, Norman, OK, Amer. Meteor. Soc., 232-234.

Zrnic, D., 1975: Simulation of weatherlike Doppler spectra and signals, *Journal of Applied Meteorology*, **14**, 4, 619-620.

_____, and S. Hamidi, 1981: Considerations for the design of ground clutter cancelers for weather radar, FAA Report, Interim Report DOT/FAA/RD-81/72, 77 pp. [Available from the National Technical Information Service, Springfield, Virginia 22161]

_____, and P. Mahapatra, 1985: Two methods of ambiguity resolution in pulse Doppler weather radars, *IEEE Trans. Aerosp. Electron. Syst.*, **AES-21**, 4, 470-483.